

Can. J. Earth Sci. Downloaded from www.nrcresearchpress.com by FA CHBEREICHSBIBLIOTHEK BUEHLPLATZ on 12/04/18  
For personal use only; this manuscript is the accepted manuscript prior to copy editing and page composition. It may differ from the final official version of record.

1  
2  
3  
4  
5  
6  
7  
8  
9  
10  
11  
12  
13  
14

Preferred orientation of ferromagnetic phases in rock-forming minerals: Insights from magnetic anisotropy of single crystals  
e-mail: ann.hirt@erdw.ethz.ch

Keywords: magnetic anisotropy, ferromagnetic inclusions, ferromagnetic exsolutions, olivine, pyroxene, amphibole, feldspar, carbonate minerals, phyllosilicate minerals

15 **Abstract:** In the early days of paleomagnetism, David Strangway was interested in understanding  
16 why igneous rocks are faithful recorders of the Earth's magnetic field. He recognized that  
17 ferromagnetic (s.l.) grains that could be discerned by optical microscopy were too large to carry a  
18 stable remanent magnetization, and speculated whether fine-grained, ferromagnetic (s.l.)  
19 inclusions or exsolutions in silicate minerals are responsible. When these inclusions or exsolutions  
20 are randomly oriented, or the silicate hosts are randomly oriented in a rock, they can be a good  
21 recorder of the field. If these minerals, however, show an alignment within the silicate host, and  
22 the host is preferentially aligned due to flow structures or deformation, then the paleomagnetic  
23 direction and paleointensity could be biased. We examine the magnetic anisotropy arising from  
24 the ferromagnetic (s.l.) phases in silicate-host minerals. Single crystals of phyllosilicate,  
25 clinopyroxene and calcite show most consistent ferrimagnetic fabric with relation to the minerals'  
26 crystallographic axes, whereas olivine and feldspar display only a weak relationship. No  
27 discernable relationship is found between the ferrimagnetic anisotropy and crystallographic axes  
28 for amphibole minerals. Our results have implications when single crystals are being used for  
29 either studies of field direction or paleointensity or in cases where silicate minerals have a  
30 preferential orientation. Phyllosilicate minerals and pyroxene should be screened for significant  
31 magnetic anisotropy.

32

### 33 **Introduction**

34           Some of the early research that David Strangway conducted was focused on understanding  
35 why volcanic rocks are good recorders of the Earth's magnetic field (Larson et al. 1969; Strangway  
36 et al. 1968). The formation of iron oxides, which serve as recorders for the Earth's magnetic field,  
37 during cooling of a magma was demonstrated by Buddington and Lindsley (1964) and Carmichael  
38 and Nicholls (1967), who investigated the role of oxygen fugacity in their formation. In studies on  
39 igneous rocks, Strangway and his collaborators noted that opaque grains, which were found in  
40 igneous rocks, were too large to carry stable remanent magnetization, i.e., be in the range of single  
41 domain. High temperature exsolution of titanomagnetite, however, led to the development of  
42 ilmenite lamellae together with magnetite. Exsolution reduces the effective particle size to the  
43 single domain range and results in an elongated shape of magnetite, which has high coercivity.  
44 Therefore, the high magnetic stability in the volcanic rocks was attributed to titanomagnetite grains  
45 that had undergone exsolution.

46           Strangway (1960) proposed also an alternative explanation for the high magnetic stability in  
47 igneous rocks, in which fine ferromagnetic (s.l.) minerals that are located within paramagnetic  
48 minerals, e.g., olivine, pyroxene, mica or feldspar, carry the stable magnetization. Ferromagnetic  
49 (s.l.) crystals can either exsolve within the paramagnetic host silicate during cooling, or become  
50 trapped during the formation of the silicate phase. The former are termed exsolutions, and form  
51 along distinct crystallographic directions or planes. The orientation of the latter is not constrained  
52 by the silicate crystal structure, and they are called inclusions. The term inclusion is also sometimes  
53 used as a generic term for both oriented exsolutions and unoriented inclusions. We will refer to  
54 ferromagnetic (s.l.) phases with a preferred orientation with respect to the silicate crystal structure  
55 as exsolutions, and use the term inclusions for randomly oriented phases incorporated during

56 crystal growth, or when it is not clear whether a ferromagnetic phase is an exsolution or inclusion.  
57 Strangway (1960) postulated that magnetite exsolutions, which formed within olivine and  
58 pyroxene crystals in diabase dikes of Precambrian age during late stage hydrothermal alteration,  
59 carry the stable remanent magnetization. Later investigations by other groups demonstrated that  
60 exsolutions can be responsible for primary magnetization in a rock (e.g., Hargraves and Young  
61 1969; Strangway 1960; Tarduno et al. 2006; Wu et al. 1974). The remanent magnetization of  
62 exsolved phases is especially stable over geologic time because they are protected against chemical  
63 alteration. Wu et al. (1974) conducted the first study in which single silicate host grains with  
64 ferromagnetic (s.l.) exsolutions were oriented and demagnetized in order to obtain the direction of  
65 the paleofield. They found cloudy feldspars contained fine grains of magnetite that carry a stable  
66 magnetization, but biotite and hornblende grains contained larger magnetite particles, whose  
67 magnetization was <sup>unstable</sup>. Later studies also found that the ferromagnetic (s.l.) exsolutions in  
68 plagioclase were more likely to fall into the single-domain size range than exsolutions in olivine,  
69 pyroxene, biotite and hornblende (Cottrell and Tarduno 1999; Dunlop et al. 2006). Bono and  
70 Tarduno (2015) used exsolutions of single domain magnetite in feldspar as a stable recorder of the  
71 Earth's magnetic field in the Ediacaran. Buchan (1979), however, who separated oriented  
72 aggregates of light and dark minerals from the Bark Lake diorite, found that feldspar carried an  
73 unstable magnetization and biotite and hornblende were more likely to carry a more stable  
74 magnetization. Tarduno et al. (2006) provides a concise overview of early petrological,  
75 paleomagnetic and rock magnetic studies on these inclusions.

76 An important aspect when using single crystals for determination of paleomagnetic  
77 directions or paleointensities, is whether these show a preferential alignment due to exsolution  
78 along specific crystallographic directions. The first study to note the preferred orientation of



79 magnetite within pyroxene was Bown and Gay (1959), who identified two preferential orientations  
80 of magnetite exsolution, which are named “Z” and “X” exsolutions. Later studies also noted a  
81 preferred alignment in both pyroxene and amphiboles (Doukhan et al., 1990; Feinberg et al., 2004;  
82 Fleet et al., 1980), Clinopyroxenes show inclusions close to the crystallographic  $[001]_{\text{cpx}}$  direction,  
83 Z inclusions, and the crystallographic  $[100]_{\text{cpx}}$  direction, X direction. Augite crystals have  
84  $[110]_{\text{mt}}//[010]_{\text{aug}}$ ,  $[111]_{\text{mt}}/(100)_{\text{aug}}$ ,  $[112]_{\text{mt}}/[001]_{\text{aug}}$  with the magnetite lattice rotated  $0.4^\circ$   
85 clockwise with respect to  $[010]_{\text{aug}}$  for the “Z”-orientation, and  $[110]_{\text{mt}}/[010]_{\text{aug}}$ ,  $[111]_{\text{mt}}/(101)_{\text{aug}}$ ,  
86  $[112]_{\text{mt}}/[101]_{\text{aug}}$  with the magnetite lattice rotated  $1.9^\circ$  anticlockwise with respect to  $[010]_{\text{aug}}$  for  
87 the “X”-orientation (Fleet et al., 1980). The exact angular rotation of the magnetite lattice in the  
88 case of pyroxene and amphibole will be dependent on the exsolution temperature (Fleet et al.,  
89 1980), but differences are small and will not affect the anisotropy tensor significantly.

90 Normally host silicates will be randomly distributed in a rock, which would mean that even  
91 if the exsolved magnetite is along preferred crystallographic directions within the silicate host,  
92 they would still be faithful recorders of the Earth’s magnetic field. If the silicate hosts, however,  
93 show a crystallographic preferred orientation, then the magnetization of the exsolved magnetite  
94 could be biased to a preferred direction, as suggested by Cottrell and Tarduno (1999). For the past  
95 fifteen years, we have been interested in determining the intrinsic anisotropy of magnetic  
96 susceptibility in common rock forming minerals (Biedermann et al. 2014a, b; 2015a, b; 2016;  
97 Martín-Hernández and Hirt 2003; Schmidt et al. 2006; 2007a). These minerals are diamagnetic or  
98 paramagnetic, and their intrinsic anisotropies have been determined using high-field torque  
99 magnetometry (Bergmüller et al. 1994), in order to isolate only the anisotropy arising from  
100 diamagnetism or paramagnetism (Martín-Hernández and Hirt 2001; 2004; Schmidt et al. 2007b).  
101 The method also isolates the ferromagnetic (s.l.) anisotropy arising from any low-coercivity

102 ferrimagnetic or high-coercivity antiferromagnetic phases within the host crystal. In this study, we  
103 report on the anisotropy of magnetic susceptibility (AMS) due to ferrimagnetic exsolutions in  
104 minerals to evaluate if there is a preferred orientation related to the crystal structure and  
105 composition of the host silicate. The high-field torsion magnetometer will only isolate a  
106 ferrimagnetic contribution if it is anisotropic. Inclusions that are randomly oriented will not  
107 contribute to the anisotropy, and thus not display any torque signal. Ferrimagnetic exsolutions  
108 were found mostly in phyllosilicate minerals, olivine, pyroxenes, amphiboles and feldspar. Some  
109 amphibole and feldspar crystals contain a high-coercivity phase, e.g. hematite, in addition to the  
110 ferrimagnetic inclusions. Carbonate minerals had little to no ferromagnetic (s.l.) phases within the  
111 crystals in general, but magnetite and hematite were found in several crystals. Rock magnetic  
112 methods were applied to aid in identification of the ferromagnetic (s.l.) inclusions.

## 113 114 **Samples and Methods**

115 Samples were in the form of single crystals and were obtained from several sources, including  
116 the ETH mineral collection, the Natural History Museum Basel, Ward's Science (USA), Siber +  
117 Siber (Switzerland), Swiss Gemmological Society or from field work. It should be noted that  
118 crystals were chosen to cover the range of their silicate chemistry and may not represent the full  
119 range of exsolution orientations and aspect ratios, which may additionally depend on the crystal's  
120 cooling history. The crystals were oriented based on their crystal habit in the case of  
121 phyllosilicates, and calcite, or Laue X-ray diffraction for olivine, pyroxene, amphibole, and  
122 feldspar crystals. X-ray diffraction was carried out at the Laboratory of Crystallography, ETH  
123 Zürich. Orient Express 3.4, a crystal orientation software, was used to process the Laue images.  
124 Further details on the samples can be found in publications that report on the paramagnetic AMS

125 of the crystals (Biedermann et al. 2014 b; 2015a, b; 2016; Martín-Hernández and Hirt 2003;  
 126 Schmidt et al. 2006; 2007a).

127 Acquisition of isothermal remanent magnetization (IRM) and magnetization curves were used  
 128 to help identify ferromagnetic (s.l.) phases in the crystals. IRM acquisition curves were either  
 129 obtained on a Princeton Measurements Corporation (PMC) magnetometer or by applying the IRM  
 130 with an ASC impulse magnetizer (Model IM-10-30) and subsequently measuring the IRM on a 3-  
 131 axis 2G Enterprises rock magnetometer. Magnetization curves were measured with a PMC  
 132 vibrating sample magnetometer or alternating gradient magnetometer. High-field torque  
 133 magnetometry was used to isolate the anisotropy arising from ferrimagnetic exsolutions in the  
 134 crystals. The torque response of the samples was measured in three mutually perpendicular planes,  
 135 by rotating the sample with 15° to 30° increments in at least four fields between 700 mT to 1800  
 136 mT. Isolation of the paramagnetic and ferrimagnetic AMS was obtained using methods described  
 137 in Martín-Hernández and Hirt (2001). It should be noted that magnetic anisotropy is described by  
 138 a symmetric second-order tensor, with its principal eigenvalues  $k_1 \geq k_2 \geq k_3$ . A torsion  
 139 magnetometer, however, only defines the deviatoric tensor, i.e., deviations from a sphere whose  
 140 diameter is the average susceptibility ( $k_{avg}$ ). Therefore, in this paper the term  $k_i$  for  $i = 1$  to 3, is  
 141 actually  $k_i - k_{avg}$ , which means that  $k_1 + k_2 + k_3 = 0$ . The shape of the anisotropy ellipsoid can be  
 142 described by the U-factor (Jelinek 1981), which can take on a value between +1 for a rotationally  
 143 oblate ellipsoid and -1 for a rotationally prolate ellipsoid, and the degree of anisotropy by the  
 144 deviatoric susceptibility  $k'$  (Jelínek 1984), where

$$145 \quad U = \frac{2k_2 - k_1 - k_3}{k_1 - k_3}$$

$$146 \quad \text{and } k' = \sqrt{[(k_1 - k_{avg})^2 + (k_2 - k_{avg})^2 + (k_3 - k_{avg})^2]}/3$$

147 or

148  $\sqrt{[(k_1)^2 + (k_2)^2 + (k_3)^2]}/3$  for the deviatoric tensor

149

## 150 **Results**

### 151 **Phyllosilicate Crystals**

152 From the original studies of Martín-Hernández and Hirt (2003) and Biedermann et al. (2014a)  
 153 a total of five biotite, eleven phlogopite, five muscovite and five chlorite crystals were evaluated.  
 154 The biotite, muscovite and chlorite crystals all showed a ferrimagnetic component to the AMS,  
 155 but only one phlogopite had a significant ferrimagnetic component (Table S1). Most of these  
 156 crystals display a paramagnetic magnetization curve, although some crystals have a closed loop,  
 157 which is weakly defined after subtracting the paramagnetic slope (cf., Martín-Hernández and Hirt,  
 158 2003). All samples, except one muscovite crystal (Mu4), however, show the acquisition of an IRM.  
 159 The coercivity of remanence ( $B_{CR}$ ) is between 12 mT and 50 mT, and the IRM is saturated by 200  
 160 mT, which indicates the presence of low coercivity minerals (Fig. 1a).

161 The paramagnetic component to the AMS of all crystals have  $k_3$  within  $9^\circ$  from the pole to  
 162 the basal plane, i.e., (001) (Martín-Hernández and Hirt, 2003), which indicates that the magnetic  
 163 fabric is controlled by the distribution of iron in the silicate sheet structure. The ferrimagnetic  
 164 component to the AMS has  $k_3$  axes well grouped for all crystals except phlogopite, but canted by  
 165 an average of  $37^\circ \pm 8^\circ$  away from (001) and towards the basal plane (Fig. 1b, c, Table S). Note  
 166 that the [100] and [010] axes were not oriented; however, individual samples were cut from larger  
 167 crystals of biotite and muscovite and have therefore similar orientations with respect to each other.  
 168 The consistent orientation of the ferrimagnetic  $k_3$  axes may indicate that their shape and orientation  
 169 is controlled by the silicate lattice, e.g. due to epitaxial growth. The shape of the ferrimagnetic  
 170 AMS ellipsoid is oblate, except for the inclusions in phlogopite, whose AMS is prolate; the degree

171 of anisotropy is very weak for all crystals. Note that the exchange of the  $k_2$  and  $k_3$  axes in  
172 phlogopite may be due to its relatively strong prolate shape.

173

## 174 **Olivine Crystals**

175 Biedermann et al. (2014b) examined the AMS on 35 natural olivine, single crystals, whereby  
176 34 of the crystals have a significant ferrimagnetic component to the high-field AMS (Table S2).  
177 Crystals often showed an open hysteresis loop after subtraction of the paramagnetic slope. The  
178 IRM of all crystals is saturated by 200 mT and  $B_{CR}$  is between 12 mT to 37 mT, which shows that  
179 only low coercivity minerals are found as ferromagnetic (s.l.) phases (Fig. 2a).

180 The orientation of the principal axes of the paramagnetic susceptibility is dependent on the  
181 iron content in the olivine structure. Pure forsterite crystals with < 1 wt % FeO appear to be  
182 isotropic. All other crystals have  $k_1$  subparallel to [001], but  $k_3$  is along [100] for forsterite crystals  
183 with 3–5 wt % FeO, and along [010] for crystals with 6–10 wt % FeO and weathered crystals with  
184 16–18 wt % FeO.

185 The ferrimagnetic contribution to the high-field AMS can vary greatly and is between 4% to  
186 87%. (Table S2). Ferrimagnetic directions do not show any strong preference in orientation with  
187 respect to the olivine lattice; however,  $k_1$  and  $k_3$  are concentrated at ca.  $45^\circ$  to [001], and  $k_2$  tend  
188 to lie in the (001) plane. The shape of the AMS ellipsoid for the ferrimagnetic component is  
189 variable and can be oblate or prolate, and the degree of anisotropy is very low in all crystals except  
190 the crystal Ol14, which has the strongest ferrimagnetic component (Table S2).

191

## 192 **Pyroxene Crystals**

193 A total of 65 single crystals were used in the study of Biedermann et al. (2015b) in their study  
194 of the AMS of clinopyroxene and orthopyroxene. From the clinopyroxene crystals, 24 augite and  
195 one diopside carry a ferrimagnetic anisotropy, and hypersthene is the only orthopyroxene sample  
196 with a significant ferrimagnetic AMS. Enstatite, most diopside crystals, aegirine, and spodumene  
197 do not display a significant ferrimagnetic component of anisotropy. IRM acquisition shows that the  
198 crystals are saturated by 200 mT for most samples, only T13 is not saturated until 1000 mT (Fig.  
199 3a).  $B_{CR}$  is between 12 mT and 46 mT, indicating a low coercivity phase, which is most likely  
200 magnetite.

201 The paramagnetic AMS was found to be related to crystalline structure and iron content. For  
202 diopside and augite, the  $k_2$  axis is subparallel to [010] of the crystal, and  $k_1$  and  $k_3$  lie in a plane  
203 containing the [100] and [001] axes. For aegirine,  $k_3$  is subparallel to (100),  $k_1$  to [001], and  $k_2$  to  
204 [010]. The hypersthene crystals consist of lamellae of orthopyroxene and Ca-rich clinopyroxene,  
205 whereby  $k_2$  and  $k_3$  lie in the lamellae plane.

206 The ferrimagnetic component of the diopside crystal, which carries a significant ferrimagnetic  
207 AMS, shows no relationship to the mineral's crystallographic axes (Table S3, Fig. 3b, c). The  
208 augite crystals, on the other hand, have a large part of their high-field AMS arising from  
209 ferrimagnetic exsolutions in the crystal. There is good grouping of  $k_3$  along the [010] axis of the  
210 crystal;  $k_1$  and  $k_2$  are also well grouped and lie in a plane containing the [100] and [001]  
211 crystallographic axes. The hypersthene crystal  $k_1$  normal to the lamellae of the ortho- and  
212 clinopyroxene (Fig. 3c, d). The degree of ferrimagnetic anisotropy is highest in the pyroxenes,  
213 compared to the other crystal groups.

214

## 215 **Amphibole Crystals**

216 A study of the paramagnetic AMS for 28 single crystals was made by Biedermann et al.  
217 (2015a). Only five crystals showed a significant component of ferrimagnetic anisotropy, one  
218 actinolite crystal (Akt1) and four hornblende samples (Amph, Amph3, NMB535 and Hbl1). From  
219 these crystals three acquired a measurable IRM (Fig. 4a). After a rapid acquisition in low fields  
220 the IRM shows a more gradual approach to saturation in comparison with other minerals.  $B_{CR}$  is  
221 relatively high, ranging from 40 mT for Amph1 to 110 mT for Akt1, which suggests the presence  
222 of a higher coercivity phase. Amph 3 also showed two sextets in Mössbauer spectroscopy,  
223 indicative of non-stoichiometric magnetite (cf. Biedermann et al. 2015a).

224 The principal axes of the paramagnetic AMS are related to the crystallographic axes of the  
225 crystal structure. For tremolite, actinolite and hornblende the paramagnetic  $k_3$  is sub-parallel to  
226 (100) crystallographic axis, and  $k_1$  is generally along [010]. Richterite has  $k_2$  along [010] and  $k_1$   
227 and  $k_3$  in a plane containing [100] and [001], whereas gedrite, which was the only orthoamphibole  
228 measured, has  $k_3$  along [100] and  $k_1$  along [001].

229 The ferrimagnetic component to the AMS is between 8% to 13% in all crystals except Amph3  
230 in which it contributes 85% to the total high-field AMS (Table S4). The directions do not display  
231 a close relationship to the crystallographic axes of the crystals, however,  $k_3$  lies generally within  
232  $20^\circ$  from the plane that contains the normal to (100) and the [010] direction (Figure 4b, c). The  
233 ferrimagnetic ellipsoids are all neutral in shape and the degree of anisotropy, as reflected by  $k'$ , is  
234 low except for NMB535.

235

### 236 **Feldspar Crystals**

237 Biedermann et al. (2016) reported on the AMS of 31 feldspar crystals with varying  
238 composition. Only eight samples possessed a significant ferrimagnetic anisotropy. These include

239 two amazonite, three orthoclase, one andesine and two sunstone crystals. The sunstone crystals  
240 contain visible, micron-sized laths of an opaque and red mineral (Fig. 5a). Two types of behaviour  
241 were found in the acquisition of IRM (Fig. 5b). One of the orthoclase and the two sunstone crystals  
242 show a rapid increase in the IRM in low fields and approach, but do not reach, saturation by 300  
243 mT.  $B_{CR}$  is between 19 mT to 40 mT. This indicates that the samples contain both low and high  
244 coercivity phases, which is further confirmed from a wasp-waisted hysteresis loop (Fig. 5 in  
245 Biedermann et al. 2016). Another orthoclase crystal and an amazonite crystal display a slower  
246 acquisition of IRM that is not saturated by 2000 mT.  $B_{CR}$  between 300 mT and 560 mT indicates  
247 the dominance of a high coercivity phase that is most likely hematite.

248 Although the high-field AMS is very weak in all crystals, the anisotropy arising from the  
249 diamagnetic susceptibility shows a relationship to the samples crystallographic axes, with the most  
250 negative susceptibility close to [010] and the least negative susceptibility along [001]. The  
251 ferrimagnetic anisotropy of the alkali feldspar crystals does not display a strong relationship to the  
252 crystallographic axes of the minerals (Fig. 5 c, d, Table S5). The  $k_2$  axes lie close to (100) for some  
253 crystals but the degree of anisotropy is extremely low. The  $k_1$  axes for the sunstone crystals,  
254 however, are along the lath direction of the ferrimagnetic exolution, which is sub-parallel to [010]  
255 (Fig. 5 e). The shape of the ferrimagnetic ellipsoid is very variable from oblate to prolate for the  
256 feldspar crystals in general, and the degree of anisotropy is the weakest compared to all other  
257 mineral types.

258

## 259 **Carbonate Minerals**

260 A systematic study of the magnetic anisotropy in carbonate minerals was carried out by  
261 Schmidt et al. (2006) on calcite and Schmidt et al. (2007a) on other carbonate minerals. Only six



262 of nineteen calcite crystals and four of 19 carbonate crystals, including one cerrusite, one dolomite,  
263 one magnesite and one rhodochrosite crystal possessed a ferrimagnetic anisotropy. Because the  
264 carbonate minerals were not oriented with respect to crystallographic axes, only the calcite crystals  
265 will be discussed. The contribution of the ferromagnetic component to the total high-field AMS is  
266 low for all crystals (Table S6).

267 IRM is acquired rapidly in low fields in most crystals (Fig. 6a). Some crystals are saturated in  
268 fields below 300 mT, whereas other crystals are not saturated at the highest applied field.  $B_{CR}$   
269 ranges between 35 and 100 mT in general. C2 is an exception with a more gradual acquisition of  
270 IRM and a  $B_{CR}$  around 600 mT (not shown). This suggests that the crystals contain a mixture of  
271 low coercivity minerals, e.g., magnetite and/or maghemite, and high coercivity minerals, most  
272 likely hematite.

273 Schmidt et al. (2006) demonstrated that the magnetic anisotropy of the non-ferrimagnetic  
274 susceptibility in the calcite crystals may be due to diamagnetism in the case that the iron content  
275 is  $< 400$  ppm at room temperature, or paramagnetic anisotropy for higher iron concentration. For  
276 the diamagnetic anisotropy  $k_3$  (most negative susceptibility) is along the [001] axis of the crystals,  
277 and for paramagnetic crystals  $k_1$  is along the [001] crystallographic axis.

278 The ferrimagnetic anisotropy has a loose group of  $k_1$  or  $k_2$  towards  $35^\circ$  and tilted about  $15^\circ$   
279 from the (001) plane (Fig. 6b). The  $k_3$  and either  $k_1$  or  $k_2$  form a girdle about this direction. This  
280 grouping is close to a cleavage plane within the crystal, which suggests that the orientation of the  
281 ferrimagnetic phases is constrained by the cleavage plane, possibly as a consequence of epitaxial  
282 growth, or growth along a crack in the crystal (Fig. 6c). The shape of the ferrimagnetic ellipsoid  
283 is generally oblate, although C4A is strongly prolate. The degree of anisotropy is relatively high  
284 compared to other crystal groups. It is more similar to augite crystals, thus reflecting control of the

285 orientation of ferrimagnetic grains by the crystal structure, which gives it a higher degree of  
286 alignment.

287

## 288 **Discussion and Conclusions**

289 Many crystals contain ferromagnetic (s.l.) exsolutions or inclusions. David Strangway's  
290 (1960) idea that ferrimagnetic minerals can reside as exsolutions within silicate minerals has been  
291 shown to be possible in many common rock-forming minerals (e.g., Bono and Tarduno, 2015;  
292 Feinberg et al., 2005; Palmer and Carmichael, 1973; Selkin et al., 2000; Smirnov et al., 2003; Usui  
293 et al., 2015; Wu et al., 1974). Inclusions are generally randomly oriented within the crystal, which  
294 means that they should not contribute strongly to any magnetic anisotropy of the crystal.  
295 Exsolutions, however, will be controlled by the crystal structure, such as cleavage or lattice planes,  
296 which will lead to a preferential alignment with respect to the host silicate. This is the case for  
297 clinopyroxene and the hypersthene crystals, in which the ferromagnetic (s.l.) contribution to the  
298 total AMS can be dominant. Preferentially oriented ferromagnetic exsolutions in pyroxenes have  
299 already been described in a number of studies (e.g., Bown and Gay, 1959; Doukhan et al., 1990;  
300 Feinberg et al., 2004; Fleet et al., 1980). The degree of this ferrimagnetic anisotropy, although  
301 weaker than what is found in a rock with texture, is relatively strong, and can contribute to the  
302 total anisotropy of the rock if the silicate crystals have a crystallographic preferred orientation. The  
303 phyllosilicate minerals have a strong cleavage related to their sheet structure, but the ferrimagnetic  
304  $k_1$  axes are tilted away from the normal to sheet structure and may reflect the stacking of the sheets.  
305 Therefore, the ferrimagnetic minerals may show an epitaxial control in growth. The other mineral  
306 whose ferromagnetic (s.l.) anisotropy is related to crystal cleavage is calcite. Both hematite and  
307 magnetite have been found to grow both on the surface and within calcite crystals. A good example

308 of hematite growth on calcite was shown by Walker et al. (1981) in the Triassic Moenkopi  
309 Formation from the Colorado Plateau.

310 Oligoclase that contains exsolutions of hematite is known as sunstone. Oligoclase has a very  
311 good {001} cleavage but also good {010} cleavage. The crystals of sunstone used in this study  
312 contained both magnetite and hematite, whereby the magnetite dominated the mineral's bulk  
313 magnetic properties. The ferrimagnetic fabric is dominated by laths of magnetite that are exsolved  
314 in the crystal cleavage and favor (010). The amazonite crystals and Orth1 have  $k_3$  close to [010]  
315 but the degree of ferrimagnetic anisotropy is very weak.

316 The  $k_1$  and  $k_3$  axes in the olivine crystals lie approximately at  $45^\circ$  from [001] in general,  
317 even though the ferromagnetic (s.l.) contribution to the high-field AMS is usually  $< 10\%$ .  
318 Biedermann et al. (2014b) speculated that there may be a mechanism that favors growth of  
319 inclusion in these directions, similar to what has been reported for Fe-Ni globules in chondritic  
320 olivine (Biedermann et al. 2014b). Further work, however, would be needed to understand this  
321 crystallographic relationship.

322 Most amphibole crystals did not contain a significant ferrimagnetic anisotropy, although it  
323 was clear that there were ferromagnetic (s.l.) inclusions in the crystals, based on their bulk  
324 susceptibility. Only five crystals possessed a ferrimagnetic anisotropy and these did not show any  
325 preference in the orientation of their principal axes.

326 The results from this study suggest that a preferred orientation of clinopyroxene,  
327 phyllosilicate and calcite minerals could lead to a preferential orientation of the ferromagnetic (s.l.)  
328 minerals in the rock if they occur as exsolutions within these minerals. The host phases can have  
329 a preferential orientation either due to emplacement of a magmatic body in the case of pyroxene,  
330 or sedimentary compaction in the case of phyllosilicate. Calcite alignment occurs usually due to

331 deformation, which would also affect the other minerals. If the ferromagnetic (s.l.) exsolutions lie  
332 in a preferred plane, then their remanent magnetization may be biased from the Earth's magnetic  
333 field direction towards the direction of their statistically aligned easy axis of magnetization. This  
334 would then give a paleomagnetic direction that does not reflect the latitude in which a rock formed  
335 or acquired its magnetization, and would also affect the intensity of magnetization. Normally,  
336 mineral alignment is not so strong as to influence the remanent magnetization of a rock as a whole,  
337 especially if other ferromagnetic (s.l.) phases are present in the rock, e.g. as individual grains. A  
338 more serious problem can occur if single crystals are being used for determination of the  
339 paleointensity of the Earth's magnetic field (cf., Selkin et al., 2000). In this case, a preferential  
340 alignment of ferromagnetic (s.l.) exsolutions would mean that the field intensity would be  
341 dependent on the direction of the ambient field with respect to a preferential orientation of the easy  
342 axes of the ferromagnetic (s.l.) phase. For this reason, it is important that any crystal that is used  
343 for paleointensity determination should be screened for any ferromagnetic (s.l.) anisotropy.

344 Strangway correctly identified ferromagnetic inclusions and exsolutions within silicates as  
345 primary remanence carriers in igneous rocks (Strangway 1960). In addition to their size (single  
346 domain range), they also have the advantage compared to individual ferromagnetic (s.l.) grains  
347 that they are protected against alteration by their host silicate. If the crystallographic lattices of  
348 silicate minerals are randomly oriented, then ferrimagnetic inclusions can be faithful recorders of  
349 the Earth's magnetic field. Problems may arise, however, when oriented exsolutions in oriented  
350 silicates are the sole remanence carriers of a rock; their anisotropy may affect the direction and  
351 intensity of magnetization. In conclusion, a better understanding of the magnetic anisotropy of  
352 ferromagnetic (s.l.) exsolutions in particular in pyroxene, phyllosilicates, some feldspars and to a  
353 lesser extent in olivine, will help make paleomagnetic studies on single crystals more robust.

354

355 **Acknowledgements**

356 We thank A. Kontny and J. Taruduno for their thoughtful comments for improving the manuscript.

357 We kindly acknowledge P. Brack, M. Schmidt, H. Mattsson, and S.A. Bosshard (ETH-Zürich), A.

358 Puschnig (Natura History Museum Basel) and A. Stucki (Siber + Siber, Aathal) for providing

359 crystals. Results from this study were supported by the Swiss National Science Foundation (SNSF)

360 under Projects: 21-50639.97, 200020-100224, 20020-143438, and 200021-129806. A.R.B. was

361 supported by SNSF Project 167609.

362

363 **References**364 Bergmüller, F., Bärlocher, C., Geyer, B., Grieder, M., Heller, F., and Zweifel, P. 1994. A torque  
365 magnetometer for measurements of the high-field anisotropy of rocks and crystals. *Meas. Sci.*  
366 *Technol.* **5**: 1466-1470.367 Biedermann, A.R., Koch, C.B., Lorenz, W.E.A., and Hirt, A.M. 2014a. Low-temperature magnetic  
368 anisotropy in micas and chlorite. *Tectonophysics* **629**: 63-74. doi:  
369 10.1016/j.tecto.2014.01.015.370 Biedermann, A.R., Koch, C.B., Pettke, T., and Hirt, A.M. 2015a. Magnetic anisotropy in natural  
371 amphibole crystals. *American Mineralogist* **100**(8-9): 1940-1951. doi: 10.2138/am-2015-  
372 5173.373 Biedermann, A.R., Pettke, T., Angel, R.J., and Hirt, A.M. 2016. Anisotropy of magnetic  
374 susceptibility in alkali feldspar and plagioclase. *Geophysical Journal International* **205**(1):  
375 479-489. doi: 10.1093/gji/ggw042.376 Biedermann, A.R., Pettke, T., Koch, C.B., and Hirt, A.M. 2015b. Magnetic anisotropy in  
377 clinopyroxene and orthopyroxene single crystals. *Journal of Geophysical Research-Solid*  
378 *Earth* **120**(3): 1431-1451. doi: 10.1002/2014jb011678.379 Biedermann, A.R., Pettke, T., Reusser, E., and Hirt, A.M. 2014b. Anisotropy of magnetic  
380 susceptibility in natural olivine single crystals. *Geochemistry Geophysics Geosystems* **15**(7):  
381 3051-3065. doi: 10.1002/2014gc005386.382 Bono, R.K., and Taruduno, J.A. 2015. Stable Earth, reversing field in the Ediacaran: A single crystal  
383 crystal study of the ca. 565 Ma Sept-iles Intrusive Suite in Laurentia. *Geology* **43**(2): 131-134.384 Bown, M. G., and Gay, P. 1959. The identification of oriented inclusions in pyroxene crystals.  
385 *American Mineralogist* **44**(5-6): 592-602.386 Buchan, K.L. 1979. Paleomagnetic studies of bulk mineral separates from the Bark Lake diorite,  
387 Ontario. *Canadian Journal of Earth Sciences* **16**(8): 1558-1565. doi: 10.1139/e79-142.388 Buddington, A.F., and Lindsley, D.H. 1964. Iron-titanium oxide minerals and synthetic  
389 equivalents. *Journal of Petrology* **5**(2): 310-357. doi: 10.1093/petrology/5.2.310.

- 390 Carmichael, I.S.E., and Nicholls, J. 1967. Iron-titanium oxides and oxygen fugacities in volcanic  
391 rocks. *Journal of Geophysical Research* **72**: 4665–4687.
- 392 Cottrell, R. and Tarduno, J.A. 1999. Geomagnetic paleointensity derived from single plagioclase  
393 crystals. *Earth and Planetary Science Letters* **169**: 1-5.
- 394 Doukhan, N., Ingrin, J., Doukhan, J.C. and Latrous, K. 1990. Coprecipitation of magnetite and  
395 amphibole in black star diopside: A 474 TEM study. *American Mineralogist* **75**(7-8): 840-  
396 846.
- 397 Dunlop, D.J., Ozdemir, O., and Rancourt, D.G. 2006. Magnetism of biotite crystals. *Earth And*  
398 *Planetary Science Letters* **243**(3-4): 805-819.
- 399 Feinberg, J.M., Wenk, H.R., Renne, P.R., and Scott, G.R. 2004. Epitaxial relationships of  
400 clinopyroxene-hosted magnetite determined using electron backscatter diffraction (EBSD)  
401 technique. *American Mineralogist* **89**(2-3): 462-466.
- 402 Feinberg, J.M., Scott, G.R., Renne, P.R., and Wenk, H.-R. 2005 Exsolved magnetite inclusions in  
403 silicates: Features determining their remanence behavior. *Geology* **33**(6): 513-516. doi:  
404 10.1130/g21290.1.
- 405 Fleet, M.E., Wilcox, G.A., and Barnett, R.L. 1980. Oriented magnetite inclusions in pyroxene from  
406 the Grenville Province. *Canadian Mineralogist* **18**: 89-99.
- 407 Hargraves, R.B., and Young, W.M. 1969. Source of stable remanent magnetism in Lambertville  
408 diabase. *American Journal of Science* **267**: 1161–1177.
- 409 Jelinek, V. 1981. Characterization of the magnetic fabric of rocks. *Tectonophysics* **79**: T63-T67.
- 410 Jelínek, V. 1984. On a mixed quadratic invariant of the magnetic susceptibility tensor. *Journal of*  
411 *Geophysics* **56**: 58-60.
- 412 Lappe, S.-C., Church, N.S., Kasama, T., Bastos da Silva Fanta, B., Bromiley, G., Dunin-  
413 Burkowski, R.E., Feinberg, J.M., Russell, S., and Harrison, R.J. 2011. 2011 Mineral  
414 magnetism of dusty olivine: A credible recorder of pre-accretionary remanence.  
415 *Geochemistry, Geophysics, Geosystems* **12**: Q12Z35. doi: 10.1029/2011GC003811.
- 416 Larson, E., Ozima, M., Nagata, T., and Strangway, D. 1969. Stability of remanent magnetisation  
417 of igneous rocks. *Geophysical Journal of the Royal Astronomical Society* **17**(3): 263-292. doi:  
418 10.1111/j.1365-246X.1969.tb00237.x.
- 419 Leroux, H.G., Libourel, L., Lamella, L., and Guyot, F. 2003. Experimental study and TEM  
420 characterization of dusty olivine in chondrites: Evidence for formation by in situ reduction.  
421 *Meteoritics and Planetary Science* **38**: 81-94. doi: 10.1111/j.1945-5100.2003.tb01047.x.
- 422 Martín-Hernández, F., and Hirt, A.M. 2001. Separation of ferrimagnetic and paramagnetic  
423 anisotropies using a high-field torsion magnetometer. *Tectonophysics* **337**(3-4): 209-221. doi:  
424 10.1016/S0040-1951(01)00116-0.
- 425 Martín-Hernández, F., and Hirt, A. 2003. The anisotropy of magnetic susceptibility in biotite,  
426 muscovite and chlorite single crystals. *Tectonophysics* **367**(1-2): 13-28. doi: 10.1016/S0040-  
427 1951(03)00127-6.
- 428 Martín-Hernández, F., and Hirt, A.M. 2004. A method for the separation of paramagnetic,  
429 ferrimagnetic and haematite magnetic subfabrics using high-field torque magnetometry.  
430 *Geophysical Journal International* **157**(1): 117-127. doi: 10.1111/j.1365-246X.2004.02225.x.
- 431 Palmer, H.C., and Carmichael, C.M., 1973. Paleomagnetism of some Grenville Province rocks,  
432 *Canadian Journal of Earth Sciences* **10**(8): 1175-1190.
- 433 Schmidt, V., Gunther, D., and Hirt, A. 2006. Magnetic anisotropy of calcite at room-temperature.  
434 *Tectonophysics* **418**(1-2): 63-73. doi: 10.1016/j.tecto.2005.12.019.

- 435 Schmidt, V., Hirt, A.M., Hametner, K., and Gunther, D. 2007a. Magnetic anisotropy of carbonate  
436 minerals at room temperature and 77 K. *American Mineralogist* **92**(10): 1673-1684. doi:  
437 10.2138/am.2007.2569.
- 438 Schmidt, V., Hirt, A.M., Rosselli, P., and Martin-Hernandez, F. 2007b. Separation of diamagnetic  
439 and paramagnetic anisotropy by high-field, low-temperature torque measurements.  
440 *Geophysical Journal International* **168**(1): 40-47. doi: 10.1111/j.1365-246X.2006.03202.x.
- 441 Selkin, P.A., Gee, J.S., Tauxe, L., Meurer, W.P., and Newell, A.J. 2000. The effect of remanence  
442 anisotropy on paleointensity estimates: a case study from the Archean Stillwater Complex.  
443 *Earth and Planetary Science Letters* **183**(3-4): 403-416.
- 444 Smirnov, A.V., Tarduno, J.A., and Pisakin, B.N. 2003. Paleointensity of the early geodynamo  
445 (2.45 Ga) as recorded in Karelia: A single crystal approach. *Geology* **31** (5): 415-418.
- 446 Strangway, D.W. 1960. Magnetic studies of some diabase dikes. *Journal of Geophysical Research*  
447 **65**(8): 2526-2526.
- 448 Strangway, D.W., Larson, E.E., and Goldstein, M. 1968. A possible cause of high magnetic  
449 stability in volcanic rocks. *Journal of Geophysical Research* **73**(12): 3787-3795. doi:  
450 10.1029/JB073i012p03787.
- 451 Tarduno, J.A., Cottrell, R.D., and Smirnov, A.V. 2006. The paleomagnetism of single silicate  
452 crystals: Recording geomagnetic field strength during mixed polarity intervals, superchrons,  
453 and inner core growth. *Reviews Of Geophysics* **44**(1).
- 454 Usui, Y., Shiuya, T., Sawaki, Y., and Komiya, T. 2015. Rock magnetism of tiny exsolved  
455 magnetite in palgioclase. from a Paleoarchean granitoid in the Pilbara craton. *Geochemistry*  
456 *Geophysics Geosystems* **16** (1): 112-115. doi: 10.1002/2014GC005508.
- 457 Wu, Y.T., Fuller, M.D., and Schmidt, V.A. 1974. Microanalysis of NRM in a granodiorite  
458 intrusion. *Earth and Planetary Science Letters* **23**: 275–285.
- 459

## 460 Figure Captions

461

462 Figure 1. a) Acquisition of IRM for selected crystals of phyllosilicate minerals; b) orientation of  
 463 the principal axes of the ferrimagnetic AMS for phyllosilicate crystals; and c) schematic  
 464 illustration of the crystal structure and preferred directions in which principal axes of the  
 465 ferrimagnetic AMS lie. All directions are shown on lower hemisphere, equal-area projection  
 466 with  $k_1$  represented by squares,  $k_2$  by triangles, and  $k_3$  by circles in this and subsequent  
 467 figures. Light grey planes or cones indicate preferred direction of the principal axes of the  
 468 ferrimagnetic AMS, in this and subsequent figures.

469

470 Figure 2. a) Acquisition of IRM for selected crystals of olivine; b) orientation of the principal  
 471 axes of the ferrimagnetic AMS (adapted from Biedermann et al., 2014b); and c) schematic  
 472 illustration of the crystal structure and preferred directions of the principal axes of the  
 473 ferrimagnetic AMS.

474

475 Figure 3. a) Acquisition of IRM for selected crystals of pyroxene; b) orientation of the principal  
 476 axes of the ferrimagnetic AMS for clinopyroxene (adapted from Biedermann et al., 2015b);  
 477 c) schematic illustration of the crystal structure and preferred directions of the principal axes  
 478 of the ferrimagnetic AMS for clinopyroxene and hypersthene composed of lamellae of  
 479 ortho- and clinopyroxene; and d) orientation of the principal axes of the ferrimagnetic AMS  
 480 for hypersthene (adapted from Biedermann et al., 2015b).

481

482 Figure 4. a) Acquisition of IRM for selected crystals of amphibole; b) orientation of the principal  
 483 axes of the ferrimagnetic AMS; and c) schematic illustration of the crystal structure.

484

485 Figure 5. a) Photomicrograph in plane light showing inclusions of magnetite/maghemite (black)  
 486 and hematite (red) with direction of  $k_1$ ; b) acquisition of IRM for selected crystals of  
 487 feldspar; c) orientation of the principal axes of the ferrimagnetic AMS from alkali feldspar  
 488 crystals; d) schematic illustration of the crystal structure and preferred directions of the  
 489 principal axes of the ferrimagnetic AMS; and e) orientation of the principal axes of the  
 490 ferrimagnetic AMS from plagioclase crystals.

491

492 Figure 6. a) Acquisition of IRM for selected crystals of carbonate minerals; b) orientation of the  
 493 principal axes of the ferrimagnetic AMS in calcite; and c) schematic illustration of the  
 494 calcite crystal structure, in which the dashed line indicates the crystallographic c-axis.

495



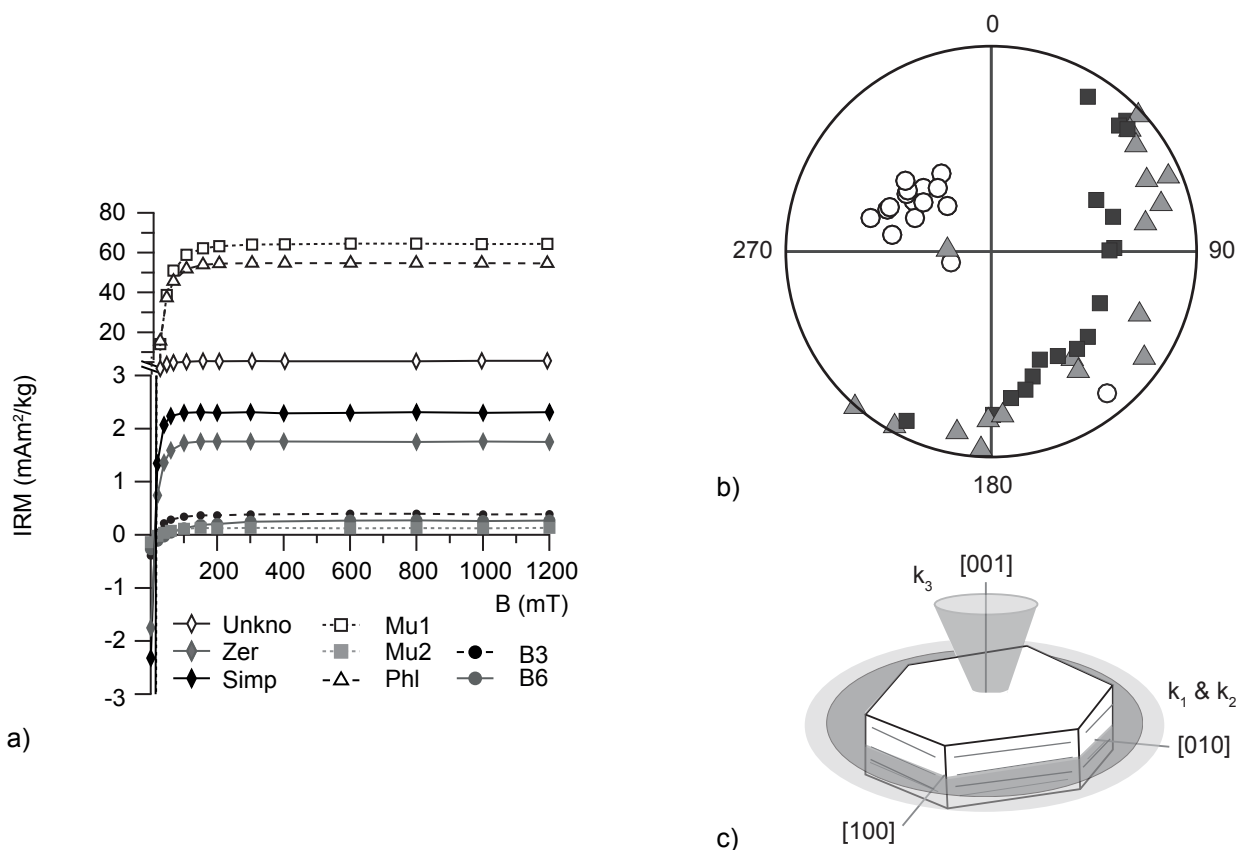


Figure 1. a) Acquisition of IRM for selected crystals of phyllosilicate minerals; b) orientation of the principal axes of the ferrimagnetic AMS for phyllosilicate crystals; and c) schematic illustration of the crystal structure and preferred directions in which principal axes of the ferrimagnetic AMS lie. All directions are shown on lower hemisphere, equal-area projection with  $k_1$  represented by squares,  $k_2$  by triangles, and  $k_3$  by circles in this and subsequent figures. Light grey planes or cones indicate preferred direction of the principal axes of the ferrimagnetic AMS, in this and subsequent figures.

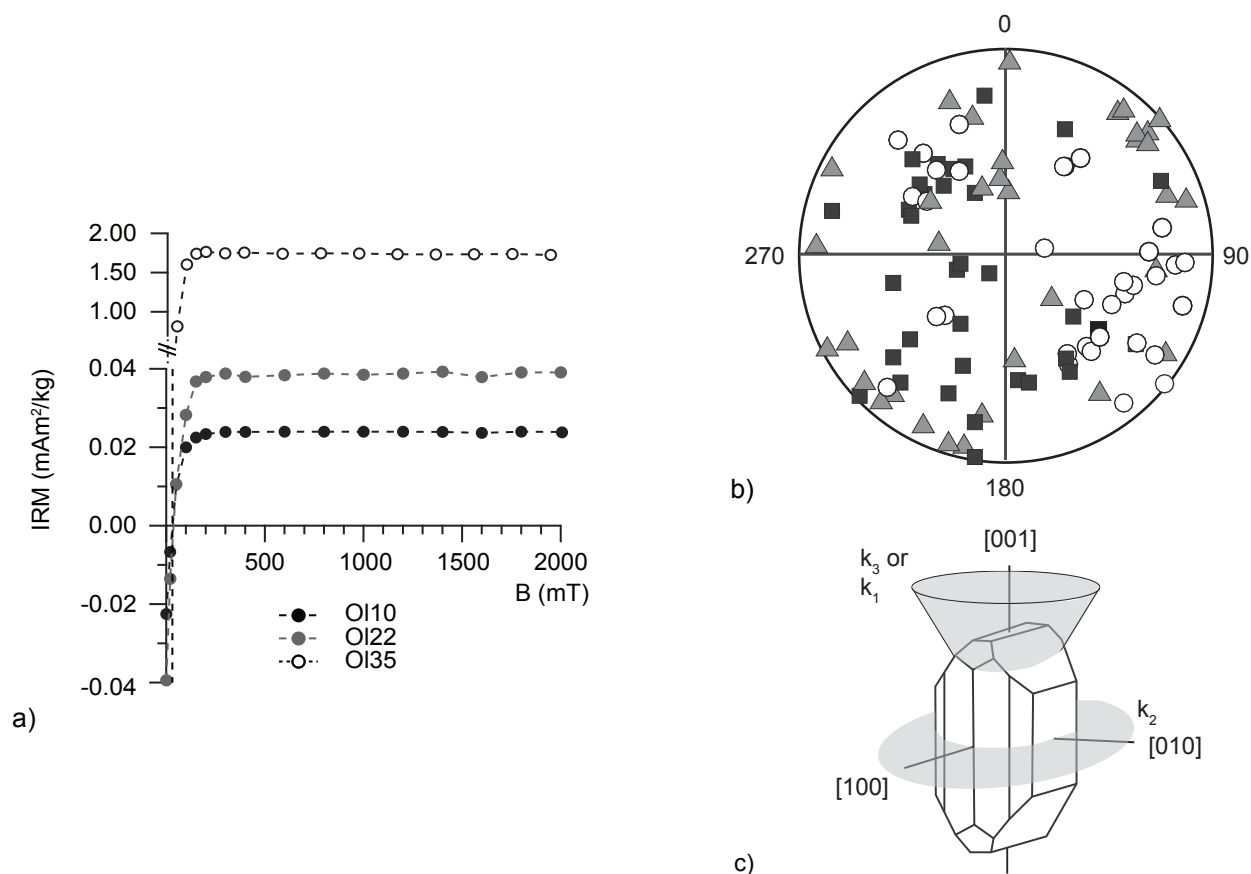


Figure 2. a) Acquisition of IRM for selected crystals of olivine; b) orientation of the principal axes of the ferrimagnetic AMS (adapted from Biedermann et al., 2014b); and c) schematic illustration of the crystal structure and preferred directions of the principal axes of the ferrimagnetic AMS.

Can. J. Earth Sci. Downloaded from www.nrcresearchpress.com by FACHBEREICHSBIBLIOTHEK BUEHLPLATZ on 12/04/18  
For personal use only. This Just-IN manuscript is the accepted manuscript prior to copy editing and page composition. It may differ from the final official version of record.

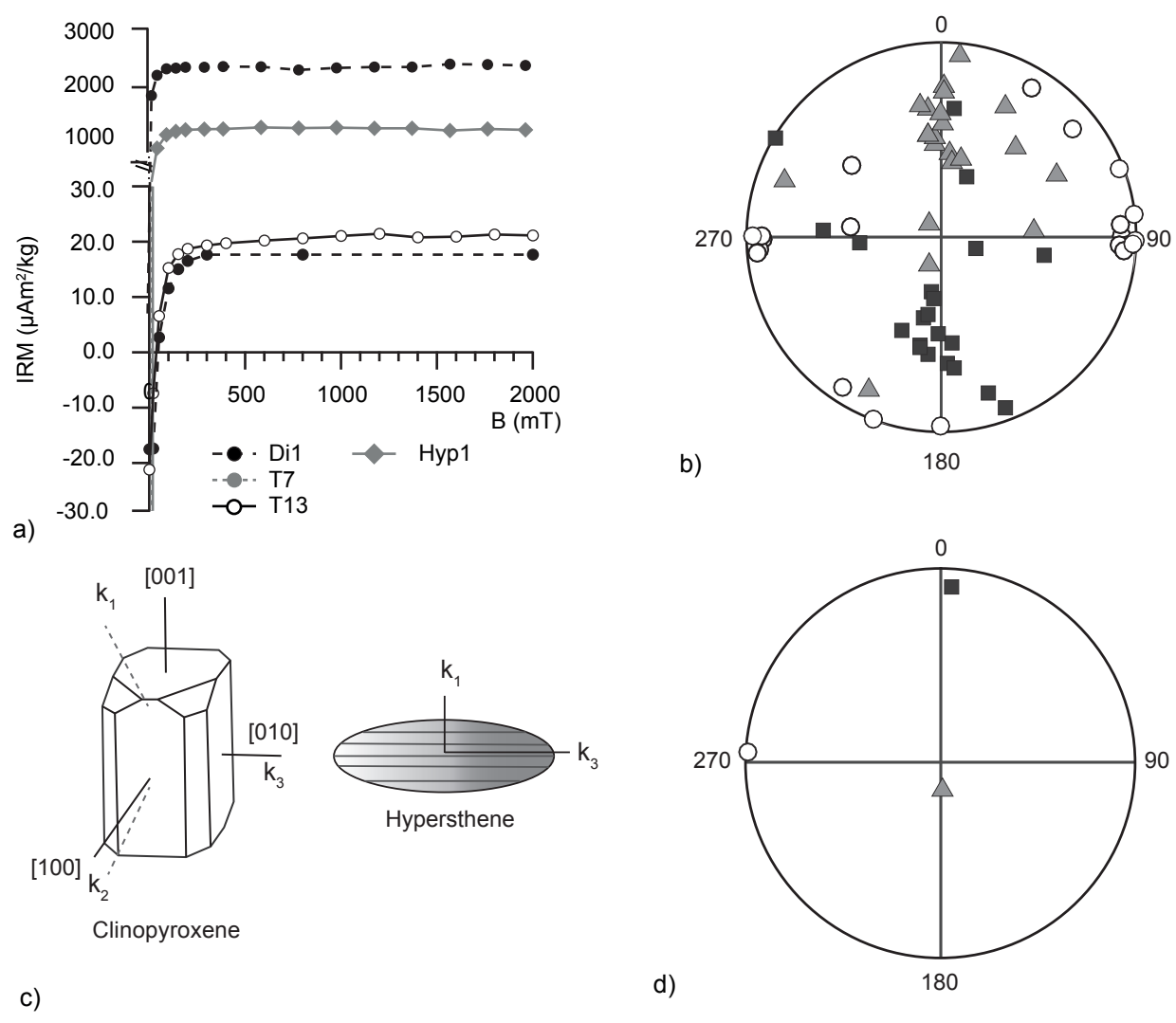


Figure 3. a) Acquisition of IRM for selected crystals of pyroxene; b) orientation of the principal axes of the ferrimagnetic AMS for clinopyroxene (adapted from Biedermann et al., 2015b); c) schematic illustration of the crystal structure and preferred directions of the principal axes of the ferrimagnetic AMS for clinopyroxene and hypersthene composed of lamellae of ortho- and clinopyroxene; and d) orientation of the principal axes of the ferrimagnetic AMS for hypersthene (adapted from Biedermann et al., 2015b).

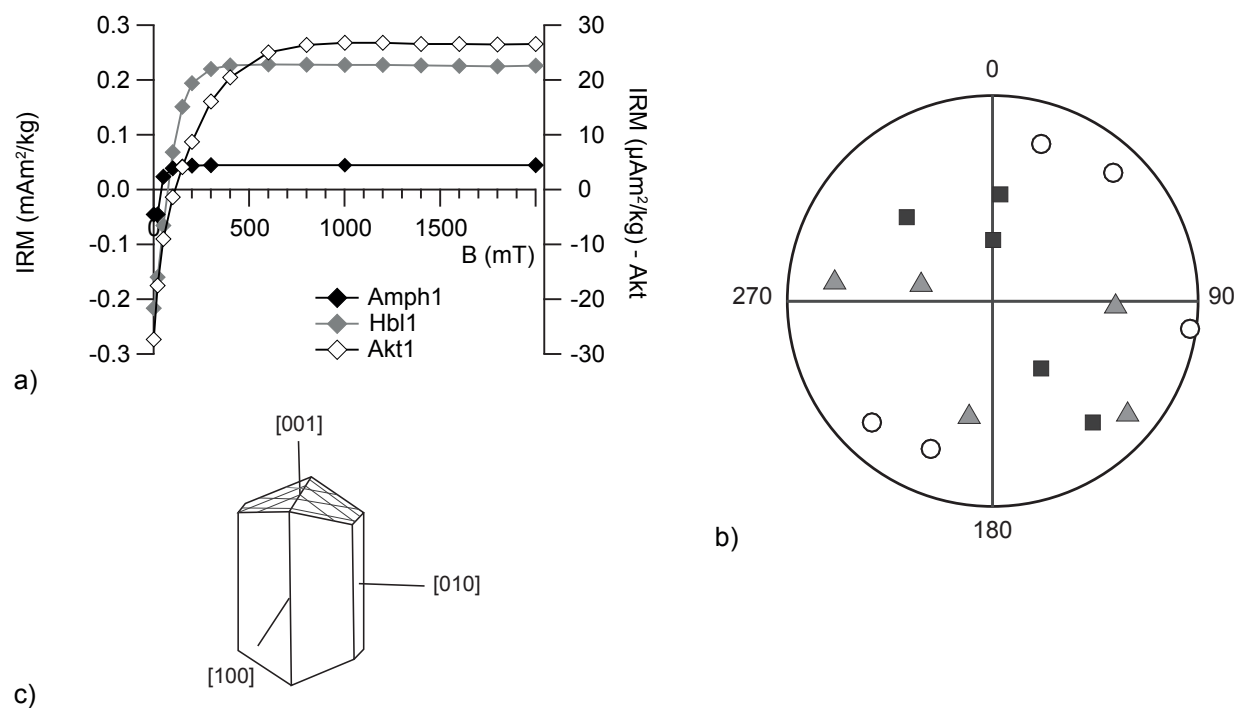


Figure 4. a) Acquisition of IRM for selected crystals of amphibole; b) orientation of the principal axes of the ferrimagnetic AMS; and c) schematic illustration of the crystal structure.

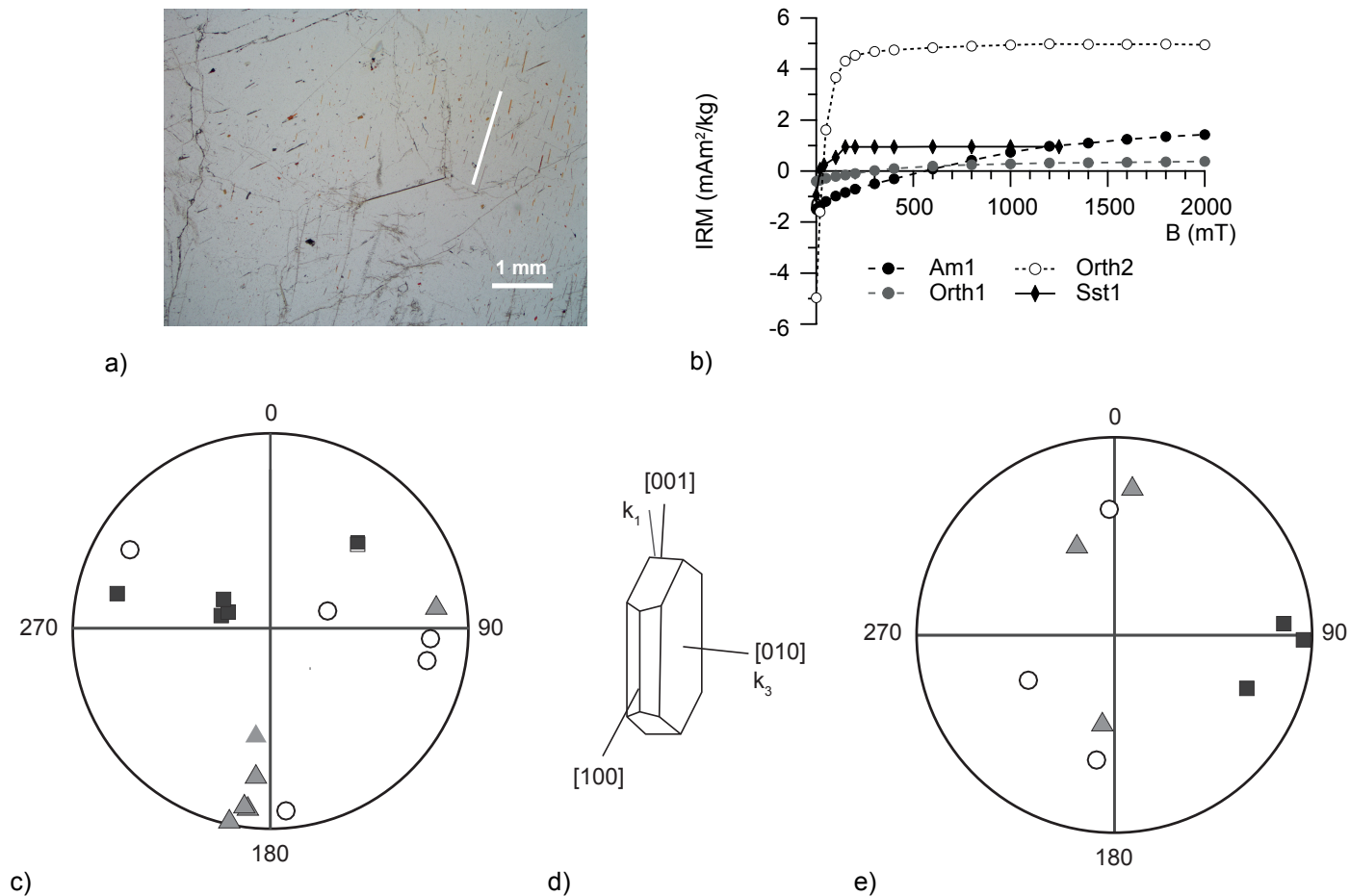


Figure 5. a) Photomicrograph in plane light showing inclusions of magnetite/maghemite (black) and hematite (red) with direction of  $k_1$ ; b) acquisition of IRM for selected crystals of feldspar; c) orientation of the principal axes of the ferrimagnetic AMS from alkali feldspar crystals; d) schematic illustration of the crystal structure and preferred directions of the principal axes of the ferrimagnetic AMS; and e) orientation of the principal axes of the ferrimagnetic AMS from plagioclase crystals.

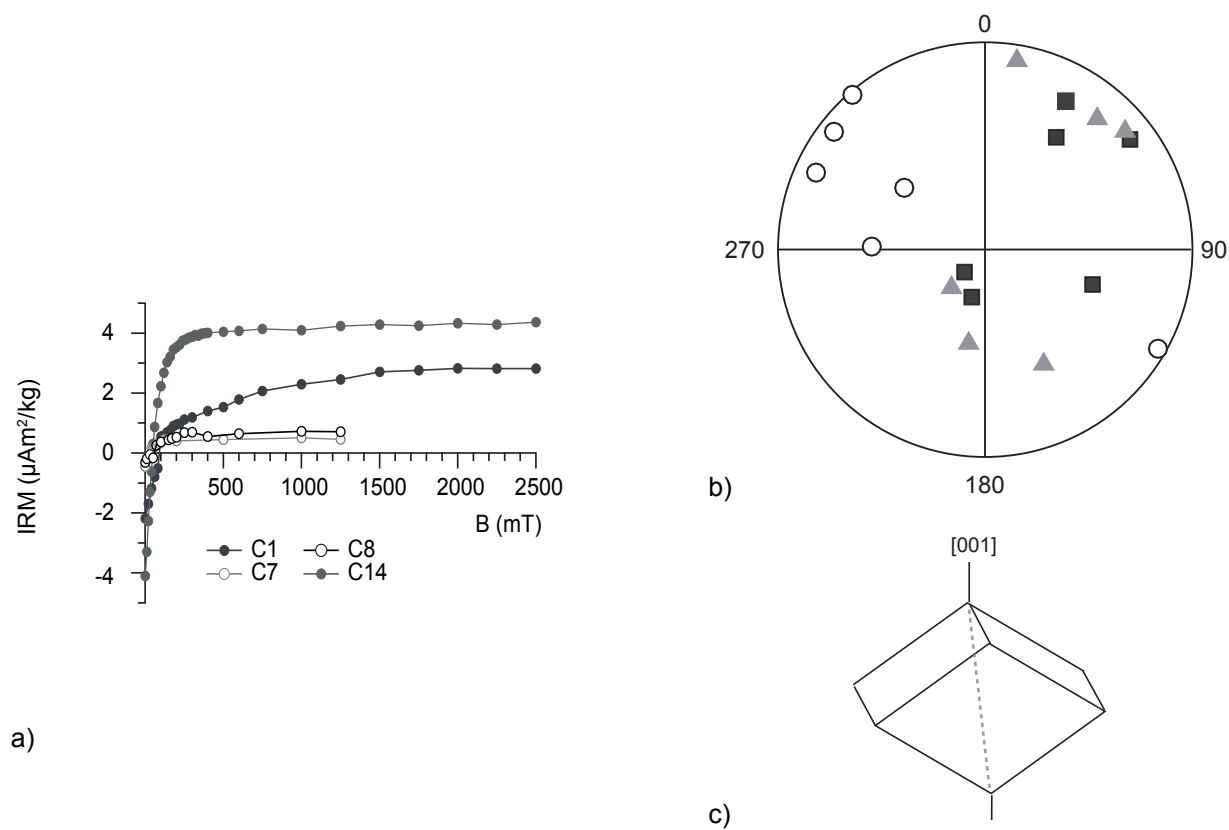


Figure 6. a) Acquisition of IRM for selected crystals of carbonate minerals; b) orientation of the principal axes of the ferrimagnetic AMS in calcite; and c) schematic illustration of the calcite crystal structure, in which the dashed line indicates the crystallographic c-axis.